APPLYING SERUM RAMAN AND FLUORESCENCE SPECTRA TO LIVER CANCER DIAGNOSIS**

Quanhong Ou [1*], Xien Yang [1], Weiye Yang [1], Liqin Jiang [1], Kai Qian [2], Youming Shi [3], Gang Liu [1*]

[1] Yunnan Key Laboratory of Opto-electronic Information Technology, School of Physics and Electronic Information at Yunnan Normal University, Kunming, China; e-mail: ouquanhong@163.com, gliu66@163.com
[2] Department of Thoracic Surgery, The First People's Hospital of Yunnan Province, Kunming, China
[3] School of Physics and Electronic Engineering at Qujing Normal University, Qujing, China

Liver cancer and healthy individual serum samples were compared based on their spectral features acquired by Raman and fluorescence spectroscopy to initially establish spectral features that can be considered spectral markers for liver cancer diagnosis. Intensity differences of the characteristic peaks of carotenes, proteins, and lipids in the Raman spectra were clearly observed in liver cancer patient serum samples compared to those of normal human serum samples. The changes in the serum fluorescence profiles of liver cancer patients were also analyzed. To probe the capacity and contrast of Raman spectroscopy as an analytical implement for the early diagnosis of liver cancer, principal component analysis was used to analyze the Raman spectra of liver cancer patients and healthy individuals. Furthermore, partial least squares-discriminant analysis was performed to compare the diagnostic performances of Raman spectroscopy for the classification of disease samples and healthy samples. Compared with existing diagnostic techniques, the Raman spectroscopy technique has many advantages such as extremely low sample requirements, ease of use, and ideal screening procedures. Thus, Raman spectroscopy has great potential for development as a powerful tool for distinguishing between healthy and liver cancer serum samples.

Keywords: *Raman spectroscopy, fluorescence spectroscopy, liver cancer, principal component analysis, partial least squares discriminant analysis.*

ПРИМЕНЕНИЕ СПЕКТРОВ КОМБИНАЦИОННОГО РАССЕЯНИЯ СВЕТА И ФЛУОРЕСЦЕНЦИИ СЫВОРОТКИ КРОВИ ДЛЯ ДИАГНОСТИКИ РАКА ПЕЧЕНИ

Q. Ou [1*], X. Yang [1], W. Yang [1], L. Jiang [1], K. Qian [2], Y. Shi [3], G. Liu [1*]

УДК 535.375.5;535.372

[1] Школа физики и электронной информации Юньнаньского педагогического университета, Куньмин, Китай; e-mail: ouquanhong@163.com, gliu66@163.com
[2] Первая народная больница провинции Юньнань, Куньмин, Китай
[3] Школа физики и электронной инженерии Педагогического университета Цюйцзина, Цюйцзин, Китай

(Поступила 16 августа 2022)

Для определения спектральных маркеров рака печени образцы сыворотки крови здоровых и больных раком печени людей сравнивали на основе их спектральных характеристик, полученных с помощью спектров флуоресценции и комбинационного рассеяния света (КР). Различия в интенсивностях характеристических пиков каротинов, белков и липидов в спектрах КР наблюдались для образцов сыворотки крови больных раком печени в сравнении с образцами сыворотки здоровых людей. Проанализированы изменения профилей флуоресценции сыворотки крови больных раком печени с ис-

** Full text is published in JAS V. 90, No. 5 (http://springer.com/journal/10812) and in electronic version of ZhPS V. 90, No. 5 (http://www.elibrary.ru/title_about.asp?id=7318; sales@elibrary.ru).

пользованием анализа главных компонент. Для исследования возможности применения КР-спектроскопии в качестве аналитического инструмента для ранней диагностики рака печени проведен анализ КР-спектров образцов сыворотки крови больных раком печени и здоровых людей методом главных компонент (PCA) и частичный дискриминантный анализ методом наименьших квадратов (PLS-DA). По сравнению с существующими методами диагностики КР-спектроскопия обладает преимуществами, такими как чрезвычайно низкие требования к образцам, простота использования и идеальные процедуры скрининга, и может быть использована в качестве инструмента для различения здоровых и пораженных раком печени образцов сыворотки крови.

Ключевые слова: *спектроскопия комбинационного рассеяния света, флуоресцентная спектроскопия, рак печени, анализ главных компонент, частичный дискриминантный анализ методом наименьших квадратов.*

Introduction. Cancer is a major public health problem worldwide [1, 2]. According to the latest data from the World Cancer Report 2020 of the International Agency for Research on Cancer (IARC), in 2020, there were 19.29 million new cancer cases worldwide, including 10.06 million males and 9.23 million females, and 905,677 new cases of liver cancer accounted for 4.7% of all the new cancers worldwide, ranking fifth. There were 9.96 million cancer deaths worldwide in 2020, including 5.53 million males and 4.43 million females; of these, 830,180 liver cancer deaths, representing 8.3% of cancer deaths, ranked third [2–5]. At present, the treatment of liver cancer still has a low radical cure rate, high recurrence rate, and poor prognosis. The main reason for the unsatisfactory efficacy of liver cancer is that the diagnosis is late. Approximately 70–80% of patients with liver cancer have reached the late stage of the disease, and effective radical treatment cannot be performed. As a result, the early diagnosis of liver cancer is extremely important [4–8]. At present, the monitoring and screening of high-risk groups are the main early diagnosis methods of liver cancer. The genetic susceptibility for liver cancer, the great differences in the morphological diversity, the micro-environment, and other factors as well as the rapid development of the disease create difficulties for the early diagnosis of liver cancer. Most patients with liver cancer are diagnosed late and are unable to be cured [5–7]. Using various tests to improve the detection rate has great significance in improving the treatment effect of liver cancer, prolonging patient life, and ensuring patient quality of life [6–9]. Currently, the traditional methods for diagnosing liver cancer include ultrasound imaging (US), computed tomography (CT), magnetic resonance imaging (MRI), and detection of serum alpha-fetoprotein (AFP) levels. However, the use of imaging to examine liver cancer is highly dependent on the experience of the operator, and it has a limited ability to distinguish liver cancer cells. A commonly used detection method to diagnose liver cancer is by detecting the serum AFP content, but the sensitivity of the AFP content is very low and cannot be the most effective means for early diagnosis [6–9]. Therefore, it is particularly important to design an economical and simple test method that can quickly and accurately detect and distinguish between early liver cancer patients and normal people. Raman and fluorescence spectroscopy techniques are potential tools for disease diagnosis. In recent years, the use of these techniques in biological studies has increased considerably, and clinical investigations relevant to cancer detection by spectroscopic means have attracted particular attention from both clinical and non-clinical researchers. Raman scattering detects the vibrational frequency of the molecular chemical bonds, and this intrinsic property causes Raman scattering to have an ultra-high chemical resolution ability. It is also important that it does not require the addition of external labels to distinguish different components and that it is a non-labeling technique [10–12]. In the medical field, the occurrence of disease often starts from subtle variations inside the molecules, which are difficult to detect by routine clinical means, such as changes in the structures of proteins, fats, sugars and nucleic acids [13–15]. However, subtle changes in the biological internal molecules can be well detected by Raman spectroscopy, thus providing great guidance and help for the early diagnosis of diseases. The Raman spectra of normal human serum (75 cases) and liver cancer serum (69 cases) were collected. The differences between the normal human and liver cancer serum spectra were analyzed, and the molecular structure changes of the main components are discussed. The effect of the fluorescence spectrum on the Raman spectra was analyzed. The Raman spectra were identified using principal component analysis (PCA) and partial least squares-discriminant analysis (PLS-DA) to facilitate the application of Raman spectra for clinical tumor diagnosis.

Materials and methods. Raman spectra were obtained by a laser microscopic confocal Raman spectrometer (ANDOR SR-500, UK). The focal length was 500 mm, a 1200 l/mm grating (Blaze 500) was used in the experiment, and the spectral resolution was 1 cm^{-1}. The laser was a 532 nm green solid-state laser (Cobolt Samba 532 nm, Cobolt AB Solna, Sweden). A thermoelectric cooled charge-coupled device (CCD)

camera was equipped with a back-illuminated, deep depletion CDD chip (Andor iDus 416, DU416A LDC-DD, Andor Technology Ltd., Belfast, UK) to collect the sample surface and scattered signals, and the camera was cooled to −70°C to reduce noise. A microscope was used (Leica DM 2700m, Leica microsystems Wetzlar GmbH) with a 50× (NA = 0.5) objective. The edge filter was used to filter stray light. Spectral data were collected using the Andor Solis software (Andor Technology). Serum samples were provided by the Department of Thoracic Surgery, the First People's Hospital of Yunnan Province. All of the participants were informed and signed consent forms for this study. Ethical approval was obtained by the Biomedical Research Ethics Committee of Yunnan Normal University (No. 2021-14). Serum samples from 69 liver cancer patients and 75 healthy subjects were collected. Sample information is listed in Table 1. Three milliliters of venous blood were drawn from each participant before breakfast and centrifuged at 3000 r/min for 20 min. Then, 1.5 mL of upper serum was collected, sealed in an Eppendorf tube, and placed in a refrigerator (temperature 4°C) for use. For the Raman spectroscopy tests, we used a pipette gun to draw 30 μL of sample and deposit it on a clean glass slide (it was soaked in aqua regia for 1 h, then washed with a large amount of ultrapure water, soaked in acetone solution for 1 h, cleaned with a large amount of ultrapure water, and then blown dry), and then it was dried in an M3 ultraclean chamber.

TABLE 1. Information about Patients with Liver Cancer and Healthy Individuals

Patient	Mean age ± SD	Sex	
		Male, *n*	Female, *n*
With liver cancer	55 ± 10	40	29
Healthy individuals	39 ± 12	44	31

The ANDOR SR-500-type Raman spectrometer laser light path was adjusted, a 532 nm excitation wavelength laser was used, and the entire experimental process was performed in the M3 ultraclean chamber laboratory. The spectra were collected by scanning for 15 s and superimposing three scans, with a spectral measurement range of 800–1800 cm^{-1}. The spectra in this range covered most of the characteristic Raman peaks of the analytes studied, with a slit width set at 100 μm and a laser power of approximately 1.16 mW on the sample. In the acquisition of the Raman spectra of the fluorescent substances, fluorescence was an important interference factor, and Raman scattering of the serum also had a certain degree of fluorescence interference. Interference caused by fluorescence occurred in the acquisition of the Raman spectra of the serum, so later, we performed fluorescence spectroscopy analysis. To eliminate the spiking effects introduced by cosmic radiation, a running median filter was applied. The entire Raman study flowchart is shown in Fig. 1.

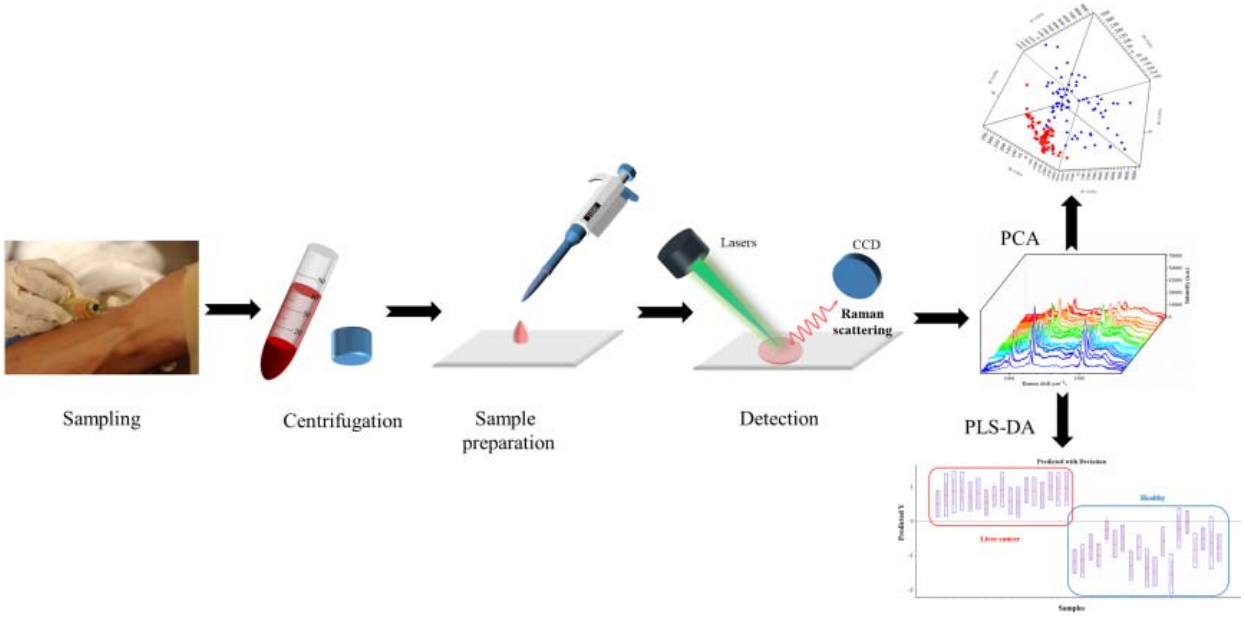

Fig. 1. Flow chart of Raman spectroscopy acquisition and analysis of serum samples.

PCA is a widely used multivariate analysis technique that can discriminate Raman spectra originating from biological systems [7, 16–22]. Two groups of spectra were simultaneously analyzed using PCA to reduce the spectral dataset to a smaller number of variables (principal components (PCs)) that describe the majority of the variance in the spectral dataset [16]. PLS-DA is a supervised classification model that was performed on the spectral data of samples from liver cancer and healthy individuals as *X*-variables (predictors) and their class information as *Y*-variables [22–26]. The second-derivative spectrum can improve the spectral resolution by amplifying small differences [6]. Second-derivative Raman spectra were obtained by the Savitzky–Golay algorithm in the OMNIC 8.2 software (Thermo Scientific). PCA and PLS-DA analysis of the second-derivative Raman spectra were performed using the Unscrambler X 10.4 software (Camo Software AS, Oslo, Norway).

Results and discussion. *Raman spectra of serum samples.* Figure 2a shows the Raman spectra of the serum samples from 75 healthy individuals. It can be seen that the peak positions of the Raman spectra were the same, and the intensity of each Raman peak changed slightly. This occurred because the experimental conditions could not be exactly the same during the test – for example, the laser power of the sample fluctuated slightly due to inconsistent focusing each time, which affected the intensity of the detection signal and moved the spectrum curve up and down. Figure 2b shows the Raman spectra of serum samples from 69 patients with liver cancer. The spectra showed that the Raman spectra of the serum samples from patients with liver cancer had the same peak positions. The Raman peak intensities of the serum from patients with liver cancer were significantly different from the characteristic peak intensities of the serum Raman spectra from normal subjects.

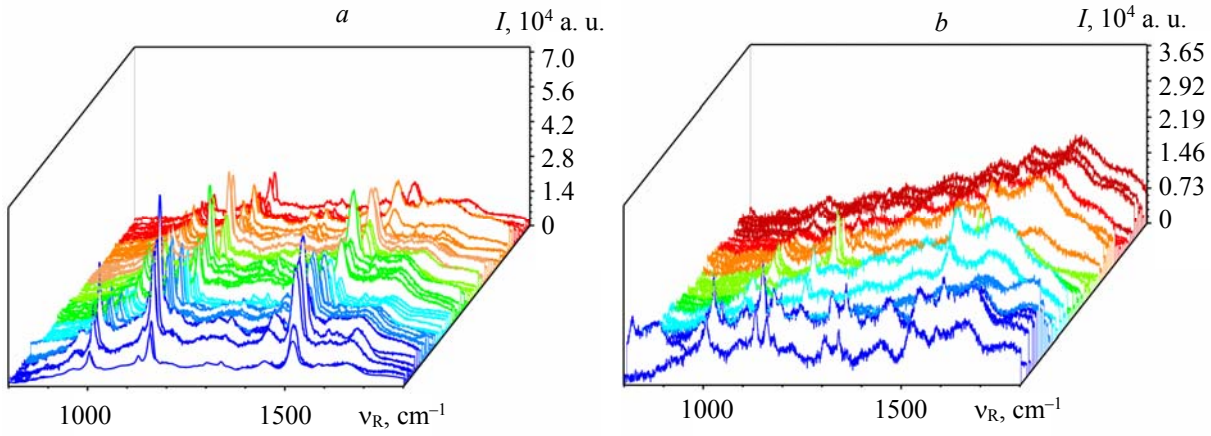

Fig. 2. Raman spectra of serum samples from 75 healthy individuals (a) and from 69 patients with liver cancer (b).

In order to compare the serum Raman spectra of patients with liver cancer and normal subjects, we averaged the spectra (Fig. 3a). Figure 3a shows that the Raman characteristic peaks of liver cancer serum and normal serum mainly occurred in the range of 600–1653 cm^{-1}. The main Raman peaks were caused by serum proteins, amino acids, lipids, sugars, carbohydrates, and other substances, which occurred in the ranges of 1003, 1127, 1156, 1301, 1337, 1447, 1519, and 1653 cm^{-1}. The peak assignments corresponding to their Raman spectra are shown in Table 2. To find the difference between the serum Raman spectra of liver cancer patients and healthy individuals, differential spectra were found by subtraction, as shown in Fig. 3b. In liver cancer patients, all the component contents were significantly reduced compared with those in healthy individuals. The three peaks with the largest differences, due to phenylalanine, protein, carotene, carotenoids, and porphyrin content variations [27], were 1003, 1156, and 1519 cm^{-1}. Two high-intensity Raman peaks at 1156 and 1519 cm^{-1} were due to the resonance Raman effect of β-carotene being strongly enhanced under excitation at 532 nm [28, 29]. The decrease in β-carotene in the diseased serum samples was consistent with previous research [29]. Weak difference peaks appeared at 962 cm^{-1} (C-O stretching of ribose) [22], 1127 cm^{-1} (C-N stretching protein), 1297 cm^{-1} (CH_2 deformation fatty acids), 1335 cm^{-1} (CH_3 CH_2 wagging, collagen (protein assignment), and nucleic acids), 1447 cm^{-1} (CH_2 CH_3 bending mode and CH_2 deformation of proteins and lipids), 1584 cm^{-1} (C=C bending mode of phenylalanine) [10], and 1653 cm^{-1} (carbonyl stretching

(C=O), C=C stretching, and protein amide I absorption) [30, 31]. Patients with malignant tumors are mostly in a high metabolic state, the amounts of protein synthesis and catabolism in the body increase, and the metabolites produced and various material components in the blood also change. Amino acids are involved in protein synthesis and catabolism, and their compositions and concentrations can reflect the metabolic state. Hyperproliferation of tumor cells causes changes in proteins, amino acids, and other components in body fluid. Rapid growth and unlimited proliferation of cancer cells require a large quantity of nutritional substrates, especially amino acids, to be consumed, inevitably leading to changes in the amino acid metabolic database of cancer tissue.

TABLE 2. Spectral Peaks and their Assignments

Peak, cm^{-1}	Vibrational mode	Major assignment
962	symmetric stretching vibration	phoisphate [10]
1003	C-C skeletal	phenylalanine [32, 10]
1127	C-N stretching [33]	protein [32]
1156	C-C, C-N stretching, in-plane vibrations of the conjugated=C-C= [34], β-carotene accumulation (C=C stretch mode) [38]	protein [32], carotenoids, most likely a cellular pigment [35–37], glycogen [39]
1297	CH_2 deformation	fatty acids
1301	C-H vibration, CH_2 twisting	triglycerides (fatty acids) [38], assign from lipid [40]
1335	CH_3CH_2 wagging	collagen (protein assignment), nucleic acid
1447	CH_2, CH_3 bending mode, CH_2 deformation	proteins & lipids [10]
1519	C=C stretch mode C-C & conjugated C=C band stretch	porphyrin, carotenoid, carotene [10]
1584	C=C olefinic stretch	protein assignment
1653	Carbonyl stretch (C=O), C=C stretch	protein amide I absorption [30, 31]

Fluorescence spectra analysis. Endogenous fluorescent substances are present in serum, such as proteins, porphyrins, carotenoids, and riboflavin, which can produce fluorescence after excitation by a certain wavelength of light [41–45]. From Fig. 3, we can find that the Raman spectral fluorescence background of the liver cancer patients was relatively strong, so we performed fluorescence spectroscopy analysis of the serum of healthy individuals and liver cancer patients.

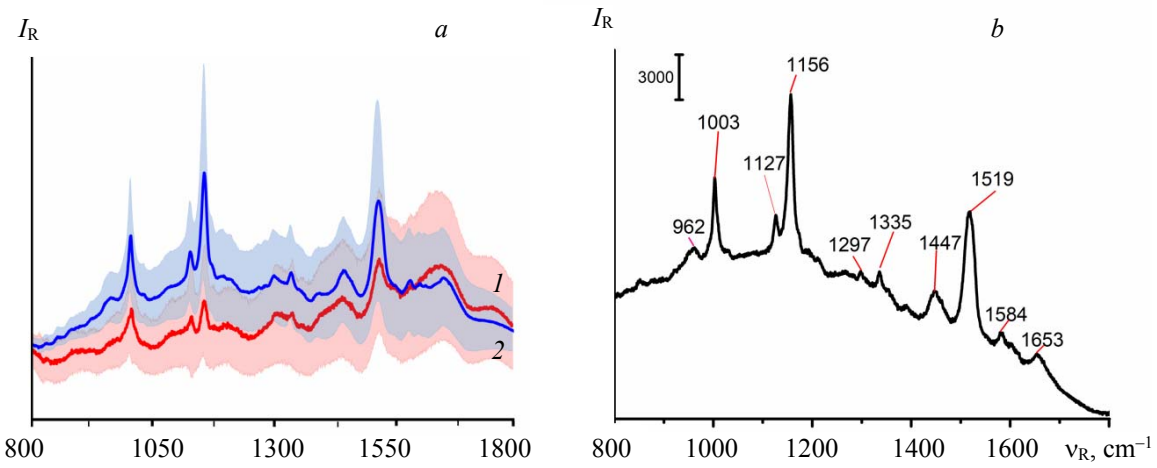

Fig. 3. (a) Average Raman spectra of serum from patients with liver cancer (line 1, $n = 69$) and healthy individuals (line 2, $n = 75$). The shaded portion indicates the standard deviation. (b) Difference spectra (absolute values of the spectra) between the spectra of liver cancer and healthy individuals.

During the experiment, 50 μL of serum samples were added to 2 mL of saline, diluted, and poured into quartz fluorescent colorimetric dishes, after which they were inserted into a fluorescent spectrophotometer (Edinburgh Instruments, FS5 type, UK, with a 150-W xenon lamp as the excitation source and a scanning speed of 60 nm/min) to obtain fluorescence spectra from the physiological saline (background spectroscopy) of liver cancer and healthy individual serum. The results are shown in Fig. 4. We can see from Fig. 4a that the fluorescence characteristic peak of physiological saline appeared at 462 nm, with porphyrin luminescence mainly present in the 600–700-nm spectral region [42]. In the spectral region with the largest difference in peak intensity between healthy individuals and liver cancer patients, the molecules playing the main luminescence role were proteins [42–46]. Proteins are formed by a peptide chain composed of multiple amino acids repeatedly folding in space, whereby the amino acids capable of fluorescing are tryptophan, tyrosine, and phenylalanine [43–44]. The growth and division of cancer cells will not be regulated by genes, and their uptake of amino acids is too fast, which disturbs the amino acid metabolism in cancer patients and eventually leads to changes in the content of amino acids in the serum [41, 45]. Compared with healthy individuals, liver cancer patients have a reduced ability to degrade aromatic amino acids, and the contents of tryptophan, tyrosine, and phenylalanine in serum are significantly increased, with increased concentrations of these three amino acids, leading to enhanced hydrogen bonding energy between light-emitting molecules [46–48].

Fluorescence spectra from healthy individual serum and liver cancer patients were used for baseline calibration, and multipeak Gaussian fitting was performed on liver cancer serum (Fig. 4b). We found that the three fitted peaks in the serum of liver cancer patients, 490, 513, and 544 nm, compared with the three peaks of healthy individuals, 490, 512, and 580 nm, were significantly different in terms of peak position and strength. In particular, the peak of the serum at 544 nm in the liver cancer patients was blue-shifted by approximately 36 nm compared with that of healthy individuals at 580 nm. This may have been due to impaired tissue and organ function in patients with malignant tumors, disrupting amino acid metabolism [45–47]. The content of luminescent amino acids in the free state was increased, and the concentration of amino acids that could emit fluorescence increased, resulting in enhanced hydrogen bond energy and elongation of the two interatomic chemical bonds that form hydrogen bonds [45–47].

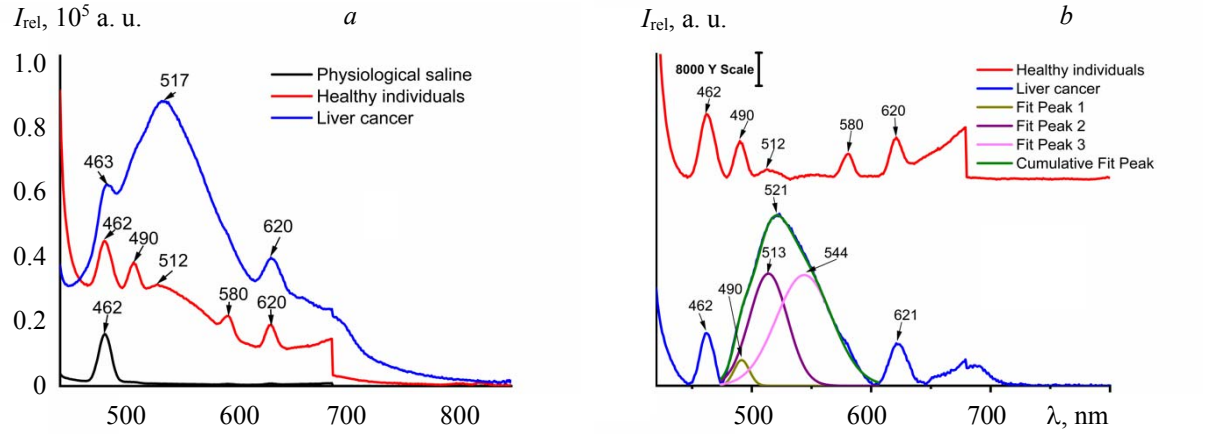

Fig. 4. (a) Fluorescence spectra of serum from healthy individuals and liver cancer patients. (b) Baseline calibration fluorescent spectra and liver cancer serum multipeak Gaussian fitting fluorescent spectra.

Principle component analysis (PCA) analysis. PCA analysis was performed on the second-derivative Raman spectra in the range of 1100–1200 cm^{-1} (Fig. 5). Figure 5a shows that the serum of patients with liver cancer was well separated from the serum samples of healthy individuals. The first three PCs explained 91% of the total variance, with 53% for PC1, 29% for PC2, and 9% for PC3. The loading plot of PCA was used to identify the peaks that had a high contribution to the differentiated samples. As shown in Fig. 5b, PC1 and PC2 mainly contributed significantly near 1127 and 1156 cm^{-1}, respectively, and these contributions were related to proteins [28] and carotenoids [34, 37, 39], respectively.

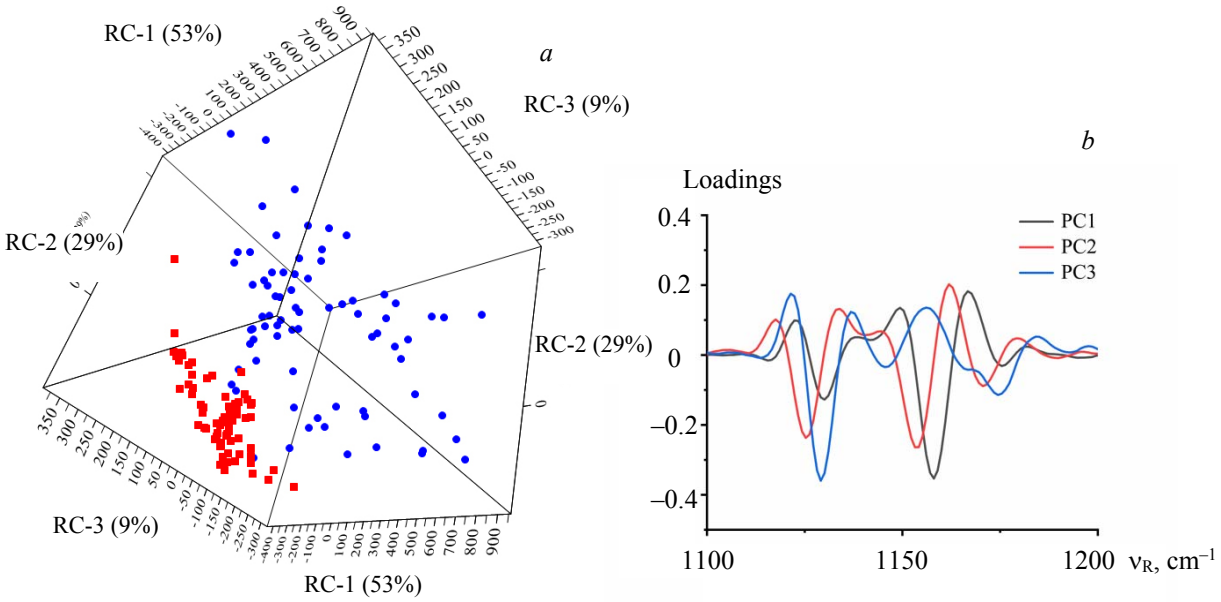

Fig. 5. Principle component analysis (PCA) analysis results in a range of 1100–1200 cm^{-1}. (a) PCA scatter plot and (b) loading plot for the second-derivative Raman spectra in the range of 1100–1200 cm^{-1}: serum from patients with liver cancer (■), serum from healthy individuals (●).

Partial least squares-discriminant analysis (PLS-DA) results. PLS-DA analysis was performed on the calibration set (patients with liver cancer provided 52 serum samples and healthy individuals provided 56 serum samples) and the validation set (patients with liver cancer provided 17 serum samples and healthy individuals provided 19 serum samples) according to the ratio of 3:1 for model work in a range of 1100–1200 cm^{-1} (Fig. 6). From Fig. 6a, we can see that the serum samples were distributed into two clusters. The red cluster was mainly composed of serum samples from patients with liver cancer, and the blue cluster was mainly composed of serum samples from healthy individuals. Fig. 6b shows the loading plot of Factor-1 and Factor-2 for identifying the peaks with high weights when classifying samples. There were positively weighted peaks at approximately 1158 cm^{-1} and passively weighted peaks at approximately 1154 cm^{-1}. The peak of this region belonged to the Raman peaks of proteins and carotenoids, thus showing that the protein and carotenoid changes during liver cancer carcinogenesis dominated in this classification model.

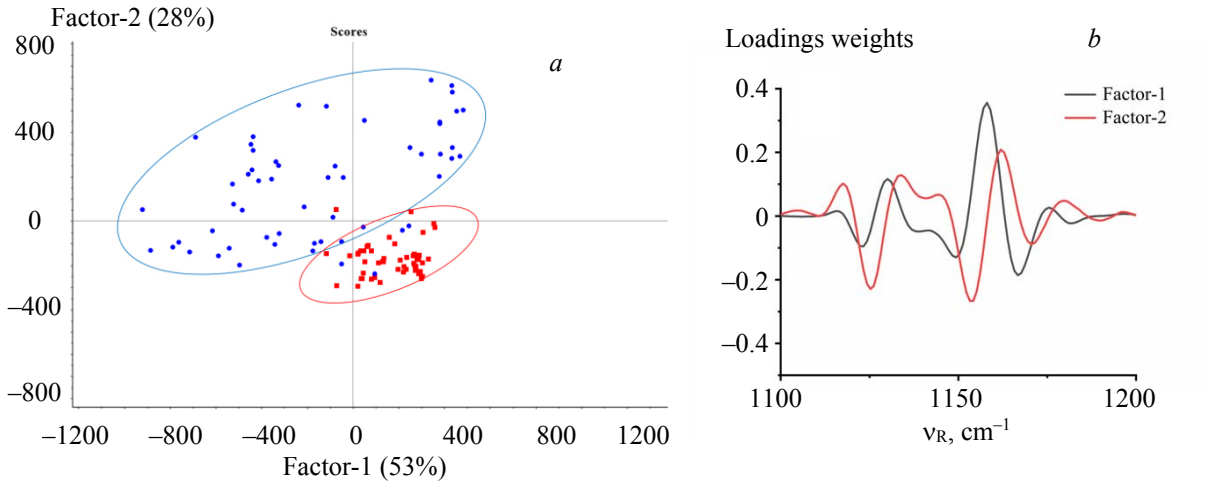

Fig. 6. Partial least squares–discriminant analysis (PLS-DA) results in the range of 1100–1200 cm^{-1}. (a) Scatter plot of PLS and (b) loading weights on the second-derivative Raman spectra in the range of 1100–1200 cm^{-1}: serum from patients with liver cancer (■), serum from healthy individuals (●).

Figure 7 shows the prediction results of the PLS-DA in the range of 1100–1200 cm^{-1}. Predicted *Y* values greater than zero were considered to correspond to liver cancer, and less than one was considered healthy. The results showed that the predicted *Y* values of 17 serum samples from patients with liver cancer and 19 serum samples from healthy individuals were consistent with the actual situation. The effect was very good, and the classification accuracy was 100%.

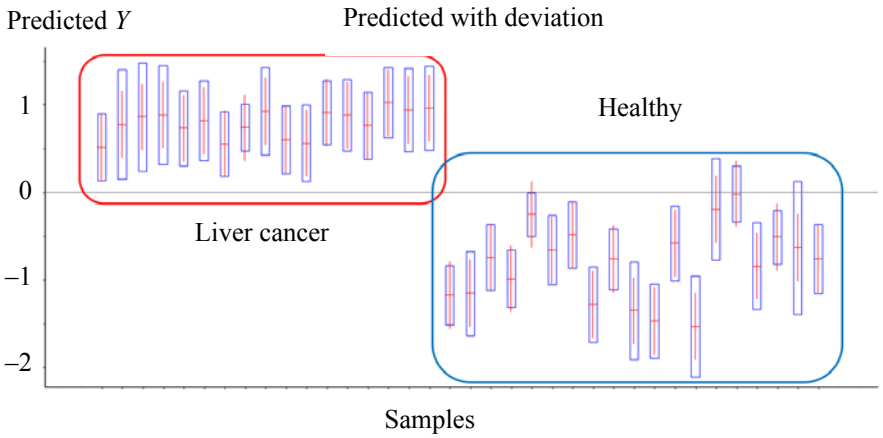

Fig. 7. Prediction results of PLS-DA in the range of 1100–1200 cm^{-1}.

Conclusions. Raman and fluorescence spectroscopy were used to classify serum samples from liver cancer and healthy individuals. The difference spectra clearly showed the changes in the various major components of the serum in the body during liver carcinogenesis. According to the fluorescence spectroscopy and Raman data analysis via PCA, the main factor causing the serum Raman spectra differences between liver cancer patients and healthy people was the changes of carotenoids and proteins in the serum. In particular, fluorescence spectroscopic analysis found that the autofluorescence amino acid content under the influence of malignant tumors increased (including tryptophan, tyrosine, and phenylalanine), which can provide a reference for clinical treatment. Using Raman spectroscopic data, a PLS-DA model was established to accurately classify serum samples from healthy individuals and liver cancer patients. Based on Raman spectroscopy, we effectively distinguished a limited sample of liver patients and healthy individuals. Although further studies are needed to clearly explain the characteristics of the Raman spectra of various serum biomolecules, the results obtained are very promising, suggesting that Raman spectroscopy can be used for clinical diagnosis. Significantly, compared with the existing diagnostic techniques, the Raman spectroscopy technique has several advantages, such as extremely low sample requirements, ease of use, and ideal screening procedure. It can provide a clear and objective result at the molecular level and help reduce human errors to a maximum extent. Thus, Raman spectroscopy has great potential to be developed as a powerful tool for distinguishing serum samples of healthy individuals and those with liver cancer.

Acknowledgments. We thank LetPub (www.letpub.com) for their linguistic assistance during the preparation of this manuscript.

This work was supported by the National Natural Science Foundation of China (Grant No. 31760341), Yunnan Fundamental Research Projects (Grant No. 202301AT070068), and Education Department Foundation of Yunnan Province (Grant No. 2022J0129).”

REFERENCES

1. R. L. Siegel, K. D. Miller, A. Jemal, *Cancer J. Clin.*, **70**, No. 1, 7–30 (2020), doi: 10.3322/caac.21590.
2. C. P. Wild, E. Weiderpass, B. W. Stewart, *World Cancer Report: Cancer Research for Cancer Prevention*, Lyon, France (2020), https://www.iarc.who.int/featured-news/new-world-cancer-report/.
3. L. A. Torre, F. Bray, R. L. Siegel, J. Ferlay, J. Lortet-Tieulent, A. Jemal, *Cancer J. Clin.*, **65**, No. 2, 87–108 (2015), doi: 10.3322/caac.21262.
4. D. Anwanwan, S. K. Singh, S. Singh, V. Saikam, R. Singh, *Biochim. Biophys. Acta (BBA) – Rev. Cancer*, **1873**, No. 1, 188314 (2020), doi: 10.1016/j.bbcan.2019.188314.

5. J. Hartke, M. Johnson, M. Ghabril, *Seminars in Diagnostic Pathology*, **34**, No. 2, 153–159 (2017), doi: 10.1053/j.semdp.2016.12.011.
6. X. Yang, Q. Ou, W. Yang, Y. Shi, G. Liu, *Spectrochim. Acta A: Mol. Biomol. Spectrosc.*, **263**, 120181 (2021), doi: 10.1016/j.saa.2021.120181.
7. K. Zhang, C. Hao, B. Man, C. Zhang, C. Yang, M. Liu, Q. Peng, C. Chen, *Vib. Spectrosc.*, **98**, 82–87 (2018), doi: 10.1016/j.vibspec.2018.07.010.
8. K. Liu, S. Jin, Z. Song, L. Jiang, L. Ma, Z. Zhang, *Vib. Spectrosc.*, **100**, 177–184 (2019), doi: 10.1016/j.vibspec.2018.12.007.
9. A. M. Lennon, A. H. Buchanan, I. Kinde, A. Warren, A. Honushefsky, A. T. Cohain, D. H. Ledbetter, F. Sanfilippo, K. Sheridan, D. Rosica, C. S. Adonizio, H. J. Hwang, K. Lahouel, J. D. Cohen, C. Douville, A. A. Patel, L. N. Hagmann, D. D. Rolston, N. Malani, S. Zhou, C. Bettegowda, D. L. Diehl, B. Urban, C. D. Still, L. Kann, J. I. Woods, Z. M. Salvati, J. Vadakara, R. Leeming, P. Bhattacharya, C. Walter, A. Parker, C. Lengauer, A. Klein, C. Tomasetti, E. K. Fishman, R. H. Hruban, K. W. Kinzler, B. Vogelstein, N. Papadopoulo, *Science*, **369**, No. 6499, eabb9601 (2020), doi: 10.1126/science.abb9601.
10. Z. Movasaghi, S. Rehman, I. U. Rehman, *Appl. Spectrosc. Rev.*, **42**, No. 5, 493–541 (2007), doi: 10.1080/05704920701551530.
11. T. Bhattacharjee, G. Maru, A. Ingle, C. M. Krishna, *J. Raman Spectrosc.*, **46**, No. 11, 1053–1061 (2015), doi: org/10.1002/jrs.4739.
12. M. Paraskevaidi, K. M. Ashton, H. F. Stringfellow, N. J. Wood, P. J. Keating, A. W. Rowbottom, P. L. Martin-Hirsch, F. L. Martin, *Talanta*, **189**, 281–288 (2018), doi: 10.1016/j.talanta.2018.06.084.
13. W. Wen, Y. Meng, J. Xiao, P. Zhang, H. Zhang, *J. Molec. Struct.*, **1038**, 35–39 (2013), doi: 10.1016/j.molstruc.2013.01.051.
14. A. F. Palonpon, J. Ando, H. Yamakoshi, K. Dodo, M. Sodeoka, S. Kawata, K. Fujita, *Nature Protocols*, **8**, 677–692 (2013), https://doi.org/10.1038/nprot.2013.030.
15. S. Pal, A. Ray, C. Andreou, Y. Zhou, T. Rakshit, M. Wlodarczyk, M. Maeda, R. Toledo-Crow, N. Berisha, J.Yang, H. T. Hsu, A. Oseledchyk, J. Mondal, S. Zou, M. F. Kircher, *Nat. Comm.*, **10**, 1926 (2019), doi: 10.1038/s41467-019-09173-2.
16. S. J. Harder, M. Isabelle, L. Devorkin, J. Smazynski, W. Beckham, A. G. Brolo, J. J. Lum, A. Jirasek, *Sci. Rep.*, **6**, 21006 (2016), https://doi.org/10.1038/srep21006.
17. S. Yan, S. Wang, J. Qiu, M. Li, D. Li, D. Xu, D. Li, Q. Liu, *Talanta*, **226**,122195 (2021), doi: 10.1016/j.talanta.2021.122195.
18. C. Zheng, S. Qing, J. Wang, G. Lü, H. Li, X. Lü, C. Ma, J. Tang, X. Yue, *Photodiagnosis and Photodynamic Therapy*, **27**, 156–161 (2019), doi: 10.1016/j.pdpdt.2019.05.029.
19. H. Wang, C. Chen, D. Tong, C. Chen, R. Gao, H. Han, X. Lv, *Photodiagnosis and Photodynamic Therapy*, **34**, 102241 (2021), doi: 10.1016/j.pdpdt.2021.102241.
20. M. Kemmlera, E. Rodner, P. Rösch, J. Popp, J. Denzler, *Anal. Chim. Acta*, **794**, 29–37 (2013), doi: 10.1016/j.aca.2013.07.051.
21. M. Cordovana, N. Mauder, M. Kostrzewa, A. Wille, S. Rojak, R. M. Hagen, S. Ambretti, S. Pongolini, L. Soliani, U. S. Justesen, H. M. Holt, O. Join-Lambert, S. L. Hello, M. Auzou, A. C. Veloo, J. May, H. Frickmann, D. Dekker, *Microorganisms*, **9**, No. 4, 853 (2021), doi: 10.3390/microorganisms9040853.
22. H. F. Nargis, H. Nawaz, H. N. Bhatti, K. Jilani, M. Saleem, *Spectrochim. Acta A: Mol. Biomol. Spectrosc.*, **246**, 119034 (2021), doi: 10.1016/j.saa.2020.119034.
23. M. Bahreini, A. Hosseinzadegan, A. Rashidi, S. R. Miri, H. R. Mirzaei, P. Hajian, *Talanta*, **204**, 826–832 (2019), doi: 10.1016/j.talanta.2019.06.068.
24. J. D. Meutter, E. Goormaghtigh, *Anal. Chem.*, **93**, No. 8, 3733–3741 (2021), doi: 10.1021/acs.analchem.0c03677.
25. L. Xia, J. Lu, Z. Chen, X. Cui, S. Chen, D. Pei, *Nanomedicine: Nanotechnology, Biology, and Medicine*, **32** ,102328 (2021), doi: 10.1016/j.nano.2020.102328.
26. K. Zhang, X. Liu, B. Man, C. Zhang, M. Liu, Y. Zhang, L. Liu, C. Chen, *Biomed. Opt. Express*, **9**, No. 9, 4345–4358 (2018), doi: 10.1364/BOE.9.004345.
27. R. Xiao, X. Zhang, Z. Rong, B. Xiu, X. Yang, C. Wang, W. Hao, Q. Zhang, Z. Liu, C. Duan, K. Zhao, X. Guo, T. Fan, Y. Zhao, H. Johnson, Y. Huang, X. Feng, X. Xu, H. Zhang, S. Wang, *Nanomedicine: Nanotechnology, Biology and Medicine*, **12**, No. 8, 2475–2484 (2016), doi: 10.1016/j.nano.2016.07.014.
28. X. Zheng, G. Wu, G. Lv, L. Yin, B. Luo, X. Lv, C. Chen, *Spectrochim. Acta A: Mol. Biomol. Spectrosc.*, **247**, 119083 (2021), doi: 10.1016/j.saa.2020.119083.

29. R. Ullah, S. Khan, F. Farman, M. Bilal, C. Krafft, S. Shahzad, *Biomed. Opt. Express*, **10**, No. 2, 600–609 (2019), doi: 10.1364/BOE.10.000600.
30. S. Farquharson, C. Shende, F. E. Inscore, P. Maksymiuk, A. Gift, *J. Raman Spectrosc.*, **36**, No. 3, 208–212 (2005), doi: 10.1002/jrs.1277.
31. C. J. Frank, R. L. Mccreery, D. C. B. Redd, *Anal. Chem.*, **67**, No. 5, 777–783 (1995), doi: 10.1021/ac00101a001.
32. J. W. Chan, D. S. Taylor, T. Zwerding, S. M. Lane, K. Ihara, T. Huser, *Biophys. J.*, **90**, No. 2, 648–656 (2006), doi: 10.1529/biophysj.105.066761.
33. R. J. Lakshmi, V. B. Kartha, C. M. Krishna, J. G. R. Solomon, G. Ullas, P. U. Devi, *Radiat. Res.*, **157**, No. 2, 175–182 (2002), doi: 10.1667/0033-7587(2002)157[0175:trsfts]2.0.co;2.
34. G. J. Puppels, H. S. P. Garritsen, J. A. Kummer, J. Greve, *Cytometry*, **14**, No. 3, 251–256 (1993), doi: 10.1002/cyto.990140303.
35. A. Mahadevan-Jansen, R. Richards-Kortum, *Proc. 19th Annual Int. Conf. IEEE Eng. Med. and Biology Soc. "Magnificent Milestones and Emerging Opportunities in Medical Engineering" (Cat. No. 97CH36136)*, **6**, 2722–2728 (1997), doi: 10.1109/IEMBS.1997.756895.
36. N. Stone, C. Kendall, J. Smith, P. Crow, H. Barr, *Faraday Disc.*, **126**, 141–157 (2004), doi: 10.1039/B304992B.
37. N. Stone, C. Kendall, N. Shepherd, P. Crow, H. Barr, *J. Raman Spectrosc.*, **33**, No. 7, 564–573 (2002), doi: 10.1002/jrs.882.
38. L. Silveira Jr., S. Sathaiah, R. A. Zângaro, M. T. T. Pacheco, M. C. Chavantes, C. A. G. Pasqualucci, *Lasers Surg. Med.*, **30**, No. 4, 290–297 (2002), doi: 10.1002/lsm.10053.
39. R. K. Dukor, *Handbook of Vibrational Spectroscopy*, John Wiley & Sons, Ltd. (2006), doi: 10.1002/0470027320.s8107.
40. R. Malini, K. Venkatakrishna, J. Kurien, K. M. Pai, L. Rao, V. B. Kartha, C. M. Krishna, *Biopolymers*, **81**, No. 3, 179–193 (2006), doi: 10.1002/bip.20398.
41. C. Guan, X. Luo, J. Lu, Z. Li, *J. Optoelectron.·Laser*, **30**, No. 2, 221–226 (2019), doi: 10.16136/j.joel.2019.02.0209.
42. J. Yu, J. Meng, Y. Li, J. Ma, R. Zheng, *Spectrosc. Spectr. Anal.*, **24**, No. 8, 981–983 (2004), doi: 10.3321/j.issn:1000-0593.2004.08.024.
43. J. R. Aibani, *J. Fluorescence*, **24**, 93–104 (2014), doi: 10.1007/s10895-013-1277-8.
44. V. Masilamani, K. Al-Zhrani, M. Al-Salhi, A. Al-Diab, M. Al-Ageily, *J. Lumin.*, **109**, No. 3-4, 143–154 (2004), doi: 10.1016/j.jlumin.2004.02.001.
45. S. Scheiner, T. Kar, J. Pattanayak, *J. Am. Chem. Soc.*, **124**, No. 44, 13257–13264 (2002), doi: 10.1021/ja027200q.
46. J. Joseph, E. D. Jemmis, *J. Am. Chem. Soc.*, **129**, No. 15, 4620–4632 (2007), doi: 10.1021/ja067545z.
47. V. Masilamani, M. S. AlSalhi, T. Vijmasi, K. Govindarajan, R. R. Rai, M. Atif, S. Prasad, A. Aldwayyan, *J. Biomed. Opt.*, **17**, No. 9, 098001 (2012), doi: 10.1117/1.JBO.17.9.098001.
48. A. C. Croce, G. Bottiroli, *Eur. J. Histochem.*, **58**, No. 4, 2461 (2014), doi: 10.4081/ejh.2014.2461.